UNIVERSITY OF CALIFORNIA
SANTA CRUZ

MODELING PROBE-BASED DATA STORAGE DEVICES

A thesis submitted in partial satisfaction of the
requirements for the degree of

MASTER OF SCIENCE

in

COMPUTER SCIENCE

by

Pu Yang

June 2000

The thesis of Pu Yang is approved:

Professor Darrell D. E. Long, Chair

Professor Tara M. Madhyastha

Professor Ali Shakouri

Professor Scott A. Brandt

Dean of Graduate Studies

Contents

List of Figures

List of Tables

Acknowledgments

I am indebted to my committee members who gave me valuable suggestions and advice. I am grateful to Darrell, my advisor, for his help and guidance throughout my graduate study at UCSC. I would like to thank Tara, who not only helps me to improve every aspect of my thesis' contents, but also to improve my writing style. I would like to thank Ali for helping me with physics and mechanics theory. Thanks also go to Scott for his insightful comments and suggestions. In addition, I thank Joel Yellin for his generous support and inputs.

Finally, I thank my parents, MeiZhen Yang and GuoZhong Cao, and my husband Zhihua for their love, support and encouragement.

Chapter 1

Introduction

For over thirty years, magnetic disks have dominated secondary storage. During this time, increases in the speeds and capacities of other systems components and the concomitant demands of these components have forced storage systems researchers to attempt to keep pace. Although efforts to increase disk performance have been successful, disks may be nearing hard limits on bit density [3].

To close this performance gap, researchers are examining a variety of new storage technologies. These technologies take varied forms, but share the common traits of high density, high throughput, and high capacity. These include holographic storage [7, 13, 14], probe-based technology based on atomic force microscopy (AFM) [4, 11], and probe-based magnetic micro-electrical mechanical systems (MEMS) storage technologies [1, 2, 5, 6, 16].

Among these new storage technologies, probe-based data storage is a promising one.

Probe-based data storage, including MEMS-based storage systems, will have fundamentally different basic abstractions from traditional rotating magnetic (and non-magnetic) media. While there are several alternative styles of probe-based storage currently being studied, all of them share some common characteristics. Probe-based storage system supports probe-based reading and writing of bits, is based on non-rotating media and initially expected to support storage densities on the order of 100 to 300 Gbit/inch^2. The storage devices are envisioned as two rectangular sleds, one with storage media and the other with a sparse array of very small read-write heads, in the range of thousands to millions. Seeks will require x and y motion of one of the sleds relative to the other. These devices are intrinsically highly parallel because some or all of the heads will be able to operate simultaneously.

Accurate models of system components, particularly performance-limiting components, are important for systems design. Disk models have been in use as long as disks, and more complicated ones simulate detailed features such as controller effects, caching, data layout, and head movement [15]. Modeling is also important for the design and development of probe-based storage devices, especially when there are no such devices available now.

The probe-based devices have physical and layout characteristics that determine their performance under given workload. The objective of this thesis is to present a model which we believe accurately describes the sled positioning, and the read/write dynamics in the probe-based storage system. Our model, which we name it as spring model, takes

the first step towards identifying the inherent relationship among various mechanical and physical factors in the system and comprehensively analyzing the sled positioning and media access using the classical theory of physics and mechanics. This model is both analytically and numerically compared with another previously proposed model by Schlosser *et al.* [16], which we call bang-bang model.[1] We demonstrate that our spring model captures important physical behaviors that are not reflected by simplifying assumptions.

The remainder of the thesis is organized as follows. Chapter 2 provides an overview of the recent development in probe-based data storage. Chapter 3 describes the bang-bang model and introduces the spring model. Chapter 4 further explores the sled movement dynamics and compares these two models. Chapter 5 describes the modeling of read/write time in the probe-based storage system. We summarizes our findings and conclude with direction for future research in Chapter 6.

[1] "Bang-bang" is a term borrowed from servo control theory.

Chapter 2

Literature Review

The mechanical operations of magnetic disks have remained almost the same over the years, although disk performance has improved dramatically. Disks consist of a collection of platters rotating on a spindle. To read and write data, the disk controller moves an arm with a read/write head to the appropriate track. Once the head is positioned, the media rotates beneath the head until the correct data is beneath it.

Probe-based storage is fundamentally different from disk storage. It consists of an array of many read/write tips over a substrate of magnetic media. These tips are very small, and are etched out entirely from silicon using a process that is compatible with standard IC lithography. Each tip, depending upon the design, may be situated on a small cantilever and can individually access data at a rate of approximately 100–200 Kbit/second.

Currently there are efforts in many research centers to study and build probe-based storage devices, most notably, Carnegie Mellon Center for Highly Integrated Information

and Storage Systems – CHI^2PS^2 [2] and IBM [4, 11].

CHI^2PS^2 is developing science and technology leading to the creation of non-volatile rewritable low-cost IC-based mass storage devices. Their research focus includes a selection of storage architectures that are compatible with IC fabrication technology. Another important aspect of their design is to integrate both storage and processing in the same chip. This incorporation can significantly improve performance, power consumption, and cost, which will result in many new applications.

CHI^2PS^2 research group has developed MEMS-based prototype probe tip and positioning system, in which the media would move in a Cartesian fashion over a very limited range of travel, and an array of thousands of microscopic read/write heads accesses the storage media in parallel. The probe-based storage system to be discussed in Chapter 3 is based upon the design at CHI^2PS^2.

Despont *et al.* [4] and Mamin *et al.* [11] discuss a new technology based upon AFM. This design, developed at IBM's Zurich Research Laboratory, proposes using tiny indentations, made in a polymer layer by AFM tips, to represent stored bits that can be read out by the same tip that wrote them. High data rates can be achieved by the parallel operation of a larger number of tiny tips in a small area. This design is believed to reach storage densities of up to 80 Gbit/cm^2, which is approximately five times greater than the expected ultimate limit for magnetic storage.

"Millipede" is the research prototype developed at the Zurich Research Laboratory. A large number of tips arranged in a two-dimensional array is scanned as a whole over a thin

polymer film that is used as storage medium. The first experimental device constructed at the laboratory consisted of 25 tips arranged in a 5×5 grid on a 25 mm^2 silicon area. The laboratory now has their second generation device, which has 1024 tips in a 32×32 array in an area of 3 mm $\times$ 3 mm. Indentation sizes and spacing reach as small as 30-40 nm which leads to high storage density.

Schlosser *et al.* [16] and Griffin *et al.* [5, 6] at School of Computer Science, Carnegie Mellon University model the data seek and access dynamics on a per request basis for a probe-based (MEMS) storage system using first-order mechanics. They discuss the design of the physical storage device, use simulations to explore how different physical characteristics impact the device's design trade-offs and performance, and describe a number of interesting architectural uses for MEMS-based storage in systems. This thesis will discuss in detail their approach in modeling the dynamics of data access and compare it with our spring model approach.

Chapter 3

Models for Probe-Based Data Storage

To make accurate decisions about data placement and scheduling, we need a model that precisely describes the seek time for probe-based storage devices. This chapter describes the design and mechanics of probe-based data storage and examine two models that rely on macroscopic physical principles: the bang-bang model and the spring model.

3.1 Device Features and Mechanics

Probe-based storage devices can be built with a variety of parameters that yield different performance characteristics. For example, we can vary the tip configuration, number of sleds, and type of media. The probe-based device discussed in this thesis is based upon the design by Carley at CHI^{2}PS^2 [2]. In this design, as shown in Figure 3.1, the probe-based storage is composed of two parts. The upper part (the gray parallelogram in the figure) is a movable sled of magnetic data, and the lower part is a fixed array of read/write

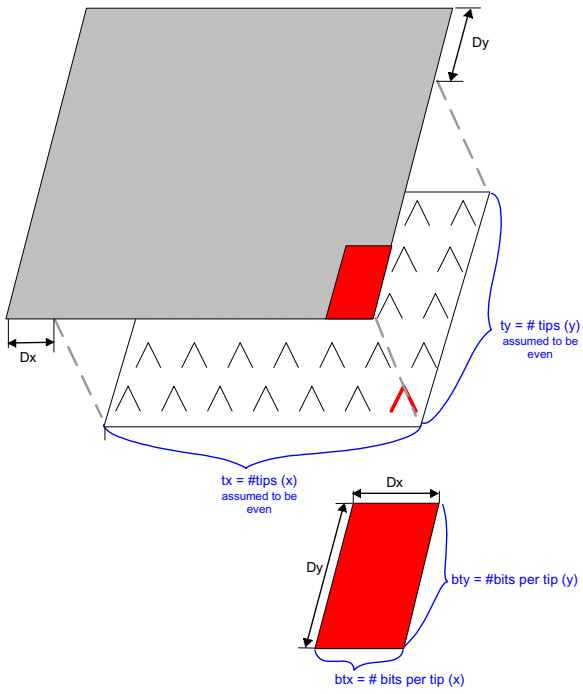

Figure 3.1: Probe-Based Storage

tips which is 100 (t_x) by 100 (t_y). The media density is 50 nm per bit. Each tip can assess data at a rate of 200 Kbit/second. The tip array is sparse, so each tip can manipulate a rectangle of bits while the sled is moving above it. This rectangle is highlighted in Figure 3.2 where D_x and D_y are the distances that one tip can access respectively.

Figure 3.2 shows an example data layout scheme. This data access pattern is based upon two assumptions: first, only one row of tips is active at a time, and second, tips are capable of reading/writing in both directions of $+y$ and $-y$. Each sector's bits are striped on the media along the x-axis, so the first bit is accessed by the first tip, the second by the second tip, etc. Thus the sector is read/written by all the tips of one row in parallel, while the sled moves above it in the y direction. After one row of tips accesses data along the

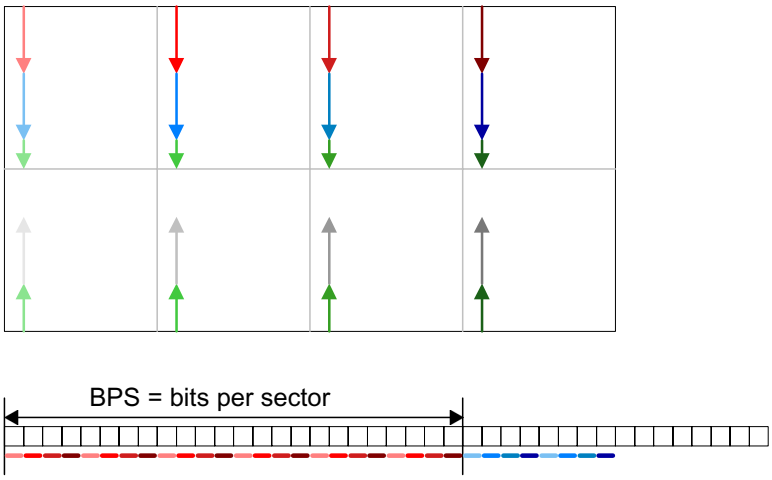

Figure 3.2: Mapping Disk Sectors to Probe-Based Storage

y-axis, the next tip row is activated and the sled reverses direction. After all the rows of tips on the chip substrate finish reading/writing a column of bits, the sled repositions to the next column which is then to be accessed. To minimize sled movement, the even rows access data in $-y$ direction, while the odd rows take the $+y$ direction.

The media sled is suspended a couple of microns above the tip substrate by silicon beams that act as springs, and moved around by forces generated by lateral resonant microactuators, as shown in Figure 3.3. In this figure, the shaded parts move and the white parts do not. Electric forces applied to the fingers of the microactuator combs exert electrostatic forces on the sled that cause it to move in the x and y direction, overcoming the forces exerted by the anchors and beams that keep it in place.

To read or write data, the sled has to be moving over the tip array at a specified velocity. Requests are queued, and after servicing one request, the sled will reposition itself so that the tip array can access the data required by the next request. This movement is called

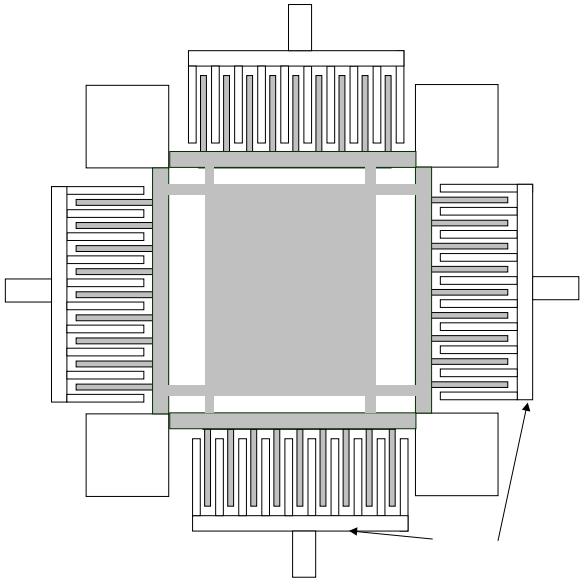

Figure 3.3: Sled and Microactuators

seek. We describe two models for this component of access time in Chapter 3. Once the sled is in position, it moves over the data with a constant velocity. The *read/write time* is a function of the sled velocity and the data layout, and is modeled separately, as described in Chapter 5.

In terms of mechanics, there are three forces working on the sled when it moves: the external electrostatic force produced by the actuator, the restoring force from the spring, and the damping (friction) force mainly from the air. Each of the three forces affects the sled movement. The electrostatic force generated by a single comb finger is expressed with the equation $F = \epsilon_0 \mathrm{V}^2(\frac{\mathrm{b}}{\mathrm{g}})$. Here ϵ_0 is the permittivity of free space, V is the applied voltage, b is the beam thickness, and g is the comb finger gap.

3.2 Bang-Bang Model

The bang-bang model, our term for the model presented in a generalized form by Schlosser *et al.* [16], describes the dynamics of the sled movement in probe-based data storage system according to Newtonian laws of mechanics. The sled movement in the bang-bang model is described by its position, velocity and acceleration. In this model, the seek time t_{seek} is decomposed into two parts: the positioning time t_{pos} and the settling down time t_{settle}. When the sleds moves from one position to another, the model assumes that it is accelerating with maximum possible acceleration to the midpoint and then decelerating the remaining half distance.

First, the calculation of positioning time t_{pos} uses the following standard formula:

$$x_{pos} = x_0 + v_0 t_{pos} + \frac{1}{2} a {t_{pos}}^2 \tag{3.1}$$

Here we get the position x_{pos} given initial position x_0, initial velocity v_0, time t_{pos}, and acceleration a. Because the bang-bang model uses constant acceleration and initial velocity of zero, we can derive the following equation for the time to reach half the distance:

$$\frac{1}{2} x_{pos} = x_0 + \frac{1}{2} a {t_{mid}}^2$$

where t_{mid} is half of the total positioning time. With $x^* = x_{pos} - x_0$, the above equation yields

$$t_{mid} = \sqrt{\frac{x^*}{a}}$$

In the bang-bang model, the total positioning time doubles the time spent on moving half

the distance. Therefore,

$$t_{pos} = 2t_{mid} = 2\sqrt{\frac{x^*}{a}} \tag{3.2}$$

The sled needs an additional time to settle down, which is the time required for the oscillation of the spring-mounted sled to damp enough for the probe tip to function. The bang-bang models assumes a constant settle down time. If including this time, we get the total seek time as proposed by the bang-bang model:

$$t_{seek} = 2\sqrt{\frac{x^*}{a}} + t_{settle} \tag{3.3}$$

Based upon Equation (3.3), the total seek time depends upon the ratio of the distance moved and the acceleration. When the sled moves a longer distance, it takes more time with a fixed. On the other hand, to move the same distance, when acceleration a is larger, it takes less time. According to Equation (3.3) other mechanical characteristics of the probe-based storage device such as spring force and damping force do not directly affect the seek time. They are absorbed by acceleration. Equation (3.3) can be used to calculate the sled's seek time in either y or x dimension. When the sled moves in both directions, the seek time is the maximum of those in x and y directions.

In practice, and as our results will show, Equation (3.3) is an aggressive assumption leading to underestimates of seek time. Acceleration is not a constant in sled movement; it changes over time. And velocity does not vary linearly over time. Besides, the bang-bang model takes constant settle down time while intuitively the seek time is substantially small when the distance moved approaches zero.

In the recent paper by Griffin *et al.* [6], the above model is modified so that the acceleration a could change along with position. It uses the piecewise-constant approximation to allow the acceleration to change according to the spring force at different positions of the sled. It breaks the whole sled's movement process into a set of smaller "chunks", with the net acceleration in each chunk being the sum of the acceleration due to the actuators and the acceleration due to the springs. This causes the acceleration to change discontinuously in the sled movement. When the number of "chunks" becomes infinitely large, this discrete modeling practice is close to a continuous version of modeling approach, which is essentially the spring model we describe in Section 3.3. This paper will focus on Equation (3.3) when talking about the bang-bang model.

We believe that the bang-bang model, while useful for understanding some of the characteristics of probe-based storage, leaves out important features of the underlying architecture. The spring model, which is to be described in Section 3.3, is based more closely upon the mechanics involved in the sled movement.

3.3 Spring Model

This section presents our approach to model the sled's movement in the probe-based storage system, which is the major contribution of the thesis. The spring model describes the dynamics of the probe-based device using classic mechanics theory. In the model, the movement of the sled is determined by the following three forces: the external force, the spring force, and the damping force. Equation (3.4) is the key equation of describing the

mechanics:

$$m\ddot{x} + \lambda\dot{x} + kx = F(t) \tag{3.4}$$

Here, x is the position of the sled at time t, m is the mass of the moving sled, λ is the damping coefficient, k is the coefficient of the elasticity of the restoring force (spring constant), and $F(t)$ is an external force.

The left-hand side of Equation (3.4) consists of three terms. The term $m\ddot{x}$ describes the movement of sled with mass m according to Newton's Second Law of Motion, where $\ddot{x}$ is the acceleration rate. The higher F is, the larger the acceleration, and vice visa. The second term $\lambda\dot{x}$ describes the impact of damping upon the movement, where $\dot{x}$ is the movement velocity. With force given, large damping or friction will lead to lower velocity. The third term of Equation (3.4), kx, is about the effect of the restoring springs which indicates that the stronger the spring is (larger k), the smaller distance the sled could move (less x) at a given level of F. For example, it is harder to compress a stronger spring.

The actual movement of the sled over time is complicated because at any time point the sled position, velocity and acceleration are determined by the above-mentioned three forces simultaneously. Solving this Equation (3.4), which is a classical second-order non-homogeneous differential equation, two steps are used according to Zeldovich *et al.* [17]. For more detailed derivation of the solution, please see Appendix A.

Section 3.3.1 and Section 3.3.2 present the two steps to derive the key Equation (3.4) and provide the insights as to how the physical and mechanical nature of the sled device

affects the whole movement process, its dynamic behavior, and seek time.

3.3.1 Solution of Spring Model with No External Force

The first step considers free oscillation, *i.e.*, the case without external force F. Equation (3.4) then becomes the homogeneous equation:

$$m\ddot{x} + \lambda\dot{x} + kx = 0 \tag{3.5}$$

It turns out that the solution to Equation (3.5) depends upon the sign of the discriminant D,

$$D = \lambda^2 - 4mk \tag{3.6}$$

When $\lambda^2 > 4mk$, the solution for Equation (3.5) is as follows:

$$x_t = C_1 e^{-at} + C_2 e^{-bt} \tag{3.7}$$

where C_1 and C_2 are constants to be determined by the initial conditions of the sled, and a and b are positive and they are functions of λ, k, and m (see Appendix A).

Solution (3.7) is applicable when there exists a strong damping force or dense friction (λ is bigger than $\sqrt{4mk}$). In this situation, the moving mass does not oscillate at all but returns to its equilibrium as quickly as possible. A typical example involving strong friction is the case that when an object is dipped into oil, the amplitude of vibration dies out exponentially as the energy of oscillation is transformed into frictional heating. However, in the probe-based data storage model, because the major damping factor is from air, the case of large damping does not apply and the sled oscillates before it finally settles down.

When $\lambda^2 < 4mk$, the general solution to the Equation (3.5) becomes:

$$x_t = C_3 e^{-rt} \cos \omega t + C_4 e^{-rt} \sin \omega t \tag{3.8}$$

where

$$r = \frac{\lambda}{2m} \tag{3.9}$$

$$\omega = \sqrt{\frac{k}{m} - \frac{\lambda^2}{4m^2}} \tag{3.10}$$

ω is defined as resonant frequency, and C_3 and C_4 are two constants to be determined by the initial condition of the sled. Equation (3.8) is different from Equation (3.7) because it includes oscillation parts $\cos \omega t$ and $\sin \omega t$.

This solution is called small damping or slight friction, in which the sled movement oscillates while it gradually moves towards the final equilibrium. The smaller λ is, the oscillation plays a bigger role during the movement. When $\lambda^2 = 4mk$, the solution is called critical damping.

3.3.2 Solution of Spring Model with External Force

The solution to the Equation (3.4) is not yet complete, because we have not considered the external force. Here we assume F is non-zero and the mechanics of the sled becomes a forced oscillation. To simplify the model, throughout this paper, the external force is assumed to be a constant during one sled movement. In other words, to move any particular distance x, F has a constant value and does not change over time. However, to move the sled to a new position, F must take on a different value.

Assuming F is independent of time t, Equation (3.4) becomes

$$m\ddot{x} + \lambda\dot{x} + kx = F \tag{3.11}$$

Equation (3.11) has a specific solution which occurs when the sled stops, namely, the sled reaches its equilibrium state. At that time both sled acceleration and velocity are zero, *i.e.*, $\ddot{x} = \dot{x} = 0$. If we define x^* as that final position that the sled settles down, Equation (3.11) becomes

$$0 + 0 + kx^* = F$$

which yields the following equation:

$$x^* = \frac{F}{k} \tag{3.12}$$

According to Zeldovich *et al.* [17], the final solution for Equation (3.11) is obtained by adding the solution of Equation (3.12) to the general solution of Equation (3.8), as given by Equation (3.13).

$$x_t = C_3 e^{-rt}\cos\omega t + C_4 e^{-rt}\sin\omega t + \frac{F}{k} \tag{3.13}$$

Here r and ω are calculated from Equation (3.9) and Equation (3.10). The constants C_3 and C_4 can be obtained by using the following two equations about the starting position x_0 and initial speed $\dot{x_0}$ of the sled:

$x_0 = C_3 + 0 + \frac{F}{k}$

$\dot{x_0} = C_3[-re^{-rt}\cos\omega t + e^{-rt}\sin\omega t(-\omega)]|_{t=0} + C_4[-re^{-rt}\sin\omega t + e^{-rt}\cos\omega t\omega]|_{t=0}$

Solution of the above system of equations is as follows:

$C_3 = x_0 - \frac{F}{k}$

$C_4 = \frac{\dot{x_0} + rC_3}{\omega}$

In this thesis we assume x_0 and $\dot{x_0}$ are zero. No generality is lost by this assumption because when the initial position is defined as zero, x is simply defined as the distance moved instead of corresponding to the real coordinates. Thus the two constants become the following:

$C_3 = -\frac{F}{k}$, and

$C_4 = \frac{rC_3}{\omega}$ where the values of r and ω can be found using Equation (3.9) and (3.10).

The behavior of x over t could take different shapes depending upon parameters, as illustrated by Figure 3.4a through 3.4d. Here we use hypothetical values only for the purpose of illustration. Figure 3.4a the case for very small damping where $m = 3 \times 10^{-4}$ kg, $\lambda = 0.1$ kg/s, $k = 700$ N/m, and $F = 700 \times 10^{-4}$ N. Because λ is small relative to k and m, the sled oscillates frequently before it finally stops. Figure 4b also uses a small damping force where $m = 3 \times 10^{-4}$ kg, $\lambda = 0.4$ kg/s, $k = 700$ N/m, and $F = 100 \times 10^{-4}$ N. The damping force in Figure 3.4b is slightly stronger compared with that of Figure 3.4a. Both Figure 3.4a and Figure 3.4b are based upon Equation (3.13). Figure 3.4c is a critical damping case, $\lambda^2 = 4mk$, $m = 12 \times 10^{-4}$ kg, $\lambda = 1.8$ kg/s, $k = 700$ N/s, and $F = 100 \times 10^{-4}$ N. Finally, Figure 3.4d that is based upon Equation (3.7) illustrates large damping in which $\lambda^2 > 4mk$, $m = 12 \times 10^{-4}$ kg, $\lambda = 2.5$ kg/s, $k = 700$ N/m, and $F = 100 \times 10^{-4}$ N. The sled does not oscillate at all but slowly converges to the new position.

Equation (3.13) is the key equation for the spring model in this paper, which is instrumental for expressing how various mechanical and physical factors affect the device functioning. It also enables us to find the velocity and acceleration rate at any t by taking first- or second- order differentiation. The velocity equation is derived as follows:

$$v_t = (\omega C_4 - rC_3)e^{-rt}\cos\omega t - (\omega C_3 + rC_4)e^{-rt}\sin\omega t$$

and the acceleration equation is as below:

$$a_t = [(r^2 - \omega^2)C_3 - 2r\omega C_4]e^{-rt}\cos\omega t + [2r\omega C_3 - (\omega^2 - r^2)C_4]e^{-rt}\sin\omega t$$

The essence of the sled movement is represented by the right-hand side of Equation (3.13), where the first two terms are oscillation parts with a constant resonant frequency ω, and the third term is based upon the final position of the sled. When t is large enough, the first two terms of Equation (3.13) become so small that the final position is solely determined by the third term.

3.3.3 Impact of Mechanical and Physical Characteristics

This section explores the relationship among various parameters and how they affect the sled movement and seek time under small damping. Their relationship is based on Equation (3.10) which computes the resonant frequency ω and Equation (3.12) which describes the sled's final equilibrium. The purpose of studying these interactions is to optimize the physical design of the storage device in order to achieve the desired level of performance.

Increase in Value	Description	x^*	ω	t
F	external force	$+$	0	$+$
k	spring coefficient	$-$	+	$-$
m	sled mass	0	$+$	$+$
λ	damping coefficient	0	$-$	$-$

Table 3.1: Impact of Parameters upon Distance Moved, Resonant Frequency, and Seek Time in the Spring Model

Table 3.1 summarizes these parameters and their impact upon oscillation frequency ω, seek time t, and distance x^*. In Table 3.1, a "$+$" indicates an increase, a "$-$" indicates a decrease, and "0" indicates no change.

First, a stronger force F will lead to a greater sled movement x^* but does not change ω, as indicated by Equation (3.10). And because the distance is longer, seek time t increases.

The spring coefficient k is closely related to both x^* and ω. If other factors are held constant, if the spring is more resilient (higher k), the sled moves less distance x^* according to Equation (3.12). A smaller x^* results in less time when other parameter values are unchanged. On the other hand, the value of the resonant frequency ω increases.

An increase in the mass of the sled m has no impact upon the distance x^* but it increases the resonant frequency ω. Because it is more difficult to change the velocity of a moving sled if it is heavier, it takes longer time to move to a new position, which results in greater seek time.

Finally, a higher damping force coefficient λ changes the dynamics of sled movement by reducing its resonant frequency ω. When the friction is intense, the sled is less likely to oscillate. Taking an extreme case as an example, when λ is large enough, the dynamics of

the sled will switch from Equation (3.8) to Equation (3.7), causing the oscillation behavior to disappear. On the other hand, change of λ does not alter the final distance moved x^*. But seek time is smaller in the oscillatory region because it is easier for the sled to settle down under stronger friction.

The foregoing analysis indicates that the impacts are multi-dimensional and vary with different parameters. In small damping, for a fixed position, if a faster reposition time is desired, we could can a lower mass m, a larger k, a greater λ, or combination of them.

The spring model addresses these parameters. Based upon the above discussions, the change of these parameters will affect the performance of probe-based storage devices, which is useful when designing such devices. However, the bang-bang model leaves out these interactive parameters when describing the physical movement of the sled in the device.

Chapter 4 will present our experiments to further understand the two models.

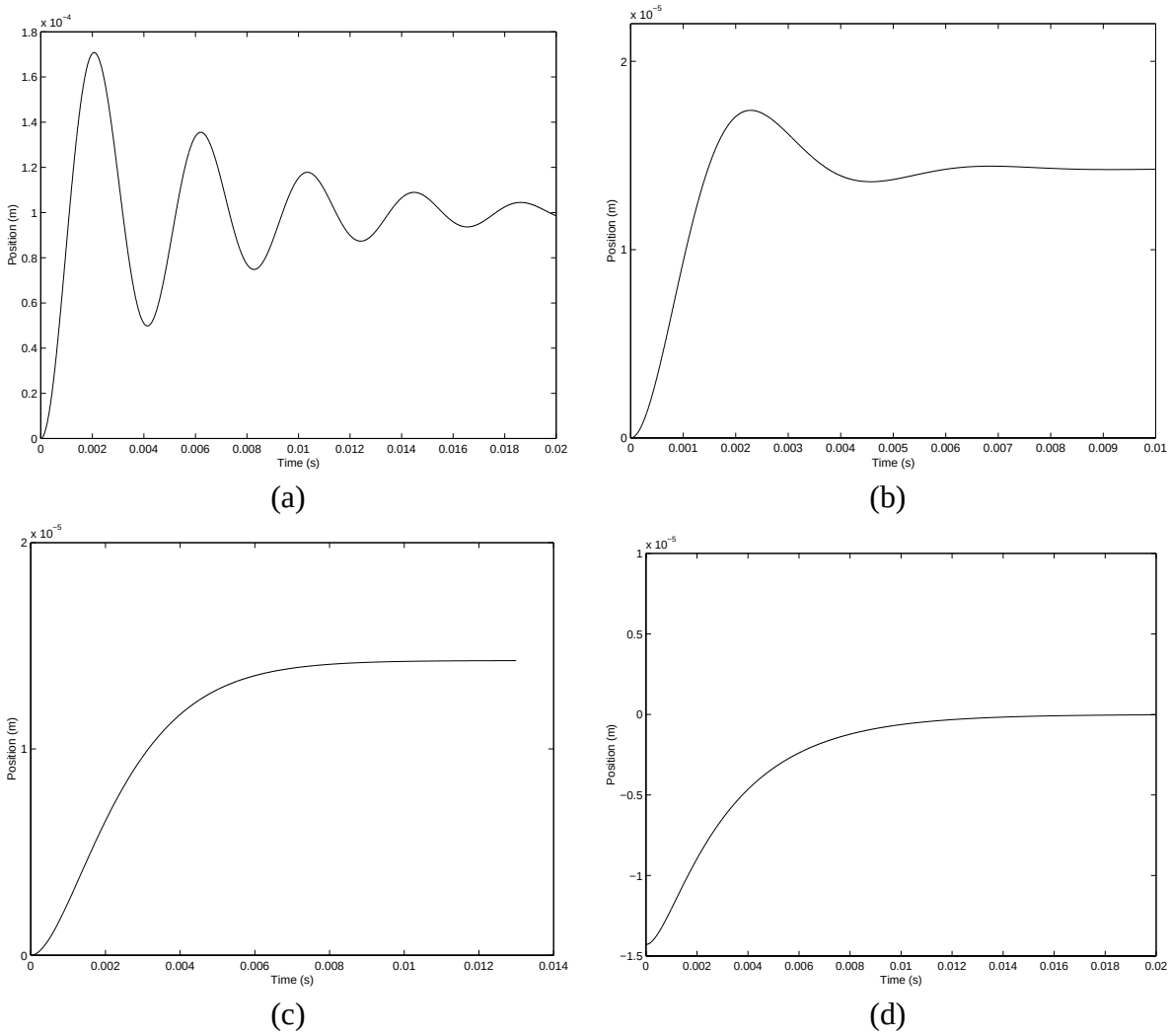

Figure 3.4: Dynamic of Sled Movement in Spring Model with Increasing Damping Force: (a) Very Small Damping ($\lambda \ll \sqrt{4mk}$); (b) Small Damping ($\lambda < \sqrt{4mk}$) (c) Critical Damping ($\lambda = \sqrt{4mk}$) (d) Large Damping ($\lambda > \sqrt{4mk}$)

Chapter 4

Numerical Simulation

Chapter 3 shows that the sled movement is a process determined by several forces and affected by various mechanical and physical characteristics. This chapter presents simulation experiments to further recognize the difference in modeling repositioning dynamics between the spring model and the bang-bang model. Experiments are taken for the purposes of computing the seek time, exploring the sensitivity to the variation of parameters, and developing further insights about the dynamics.

4.1 Experiment Design

The key equations used to calculate the seek time are Equation (3.3) for the bang-bang model and Equation (3.13) for the spring model. These two equations involve two different sets of parameters, which makes numerical comparison difficult. For example, for a given acceleration, the final distanced moved x^* is changing in the bang-bang model

but not in the spring model. We make the comparison consistent by applying the inherent relationship among various parameters.

First, we choose a series of x^* that the sled is going to reach. In the bang-bang model, the calculation of the seek time is straightforward as Equation (3.3) can be analytically applied with given x^*. However in the spring model, the dynamics equation does not directly involve x^* but we could vary F to get each value of x^* based upon Equation (3.12). Because when the final distance is chosen, the force needed is determined by Equation (3.12) in the spring model. Each obtained F is then plugged into Equation (3.13) to calculate the dynamics of x_t and then calculate the seek time.

Given x_t, a numerical solution is used, which regenerates the dynamics of x against time t. By plotting x against t and imposing a tolerance range, we can calculate the seek time.

It is necessary for the spring model to set a tolerance range because with the presence of restoring and damping forces, the sled is continuously oscillating, though the amplitude is decreasing. We say the sled stops when its oscillation amplitude no longer exceeds a pre-specified range, called tolerance. Because the distance between two neighboring bits is 50 nm, we choose a tolerance value as $\pm$25 nm. When recording the change of x along with t in the simulation, we keep the most recent time when x is still outside the tolerance range, which helps us to determine how long it takes the sled to settle down.

Parameter	Description	Values
m	mass	$(1, 2, 3) \times 10^{-4}$ kg
F	external force	$(0, 10, 20, \ldots, 500) \times 10^{-4}$ N
k	spring coefficient	$300, 500, 700$ N/m
λ	damping coefficient	$0.445, 0.482, 0.626, 0.743, 0.763$ kg/s
ω	resonant frequency	220 Hz
a	acceleration	115 m/s^2
t_{settle}	settle down time	1.447 ms

Table 4.1: Parameter Values in the Simulation

4.2 Choice of Parameter Values

Table 4.1 summarizes the parameters and their value ranges adopted in the thesis. First, the value for m is approximated according to the size of the sled. Because the polysilicon density for the sled is 2.3 g/cm^3, m for the moving media sled is 2.3×10^{-4} kg ($2.3 \times 10 \times 10 \times 1 \times 10^{-6}$) if the sled has the dimensions: length (1 cm), width (1 cm) and height (1 mm). The size of sled can vary and so does the mass. Therefore we choose the following three reasonable values for mass m in the experiments: 1×10^{-4} kg, 2×10^{-4} kg and 3×10^{-4} kg.

Once we know m and a, force F is determined by

$$F = ma \tag{4.1}$$

Schlosser *et al.* [16] sets the acceleration a 115 m/s^2. If m is 2×10^{-4} kg, F is 230×10^{-4} N ($115 \times 2 \times 10^{-4}$). This is an approximate and we allow F to vary in our experiments to explore the effect of different F upon the dynamics. F ranges from a minimum of zero to a maximum of 500×10^{-4} N which roughly doubles the estimate of 230×10^{-4} N.

The spring constant k is chosen according to sled's final equilibrium equation (3.12), which determines the value of k given F and x^*. The maximum length that a sled can move is about 100 μm according to Schlosser *et al.* [16] and Carley [2]. Thus we can have an idea about possible values for k. Assuming F is 230×10^{-4} N and x^* is 50 μm, k is 460 N/m. This is one reasonable estimate. However, we determine the range of values used in this experiment by looking at how realistic the seek time is. We wish to limit the seek time to several milliseconds at most. If k becomes too small compared with the external force F, the sled will spend a lot of time oscillating and the seek time will be too long. Therefore, we vary k in the experiments from 300, 500, to 700 N/m.

In the spring model, λ is set through the following two methods. First, according to the frequency equation (3.10), λ is calculated from the values of m, k, and ω. Schlosser *et al.* [16] points out that ω is 220 Hz in their first generation model, which is consistent with the x-dimension settling down time of 1.447 ms. The same frequency of 220 Hz is used for the two models, which results in the value of 0.626 kg/s for λ, given $k = 500$ N/m and $m = 2 \times 10^{-4}$ kg respectively.

The second method of determining λ is by looking at Equation $D = \lambda^2 - 4mk$. With small damping, i.e., $\lambda^2 - 4mk < 0$, then given $m = 2 \times 10^{-4}$ kg and $k = 500$ N/m, λ should be less than 0.632 kg/s ($\sqrt{4 \times 2 \times 10^{-4} \times 500}$). Both methods suggest that λ should be around 0.6 kg/s or smaller, with the upper limit depending upon m and k. Therefore, throughout the experiments, λ is calculated from Equation (3.10). When using the default value of mass $m = 2 \times 10^{-4}$ kg, it is to take the following three values: 0.482

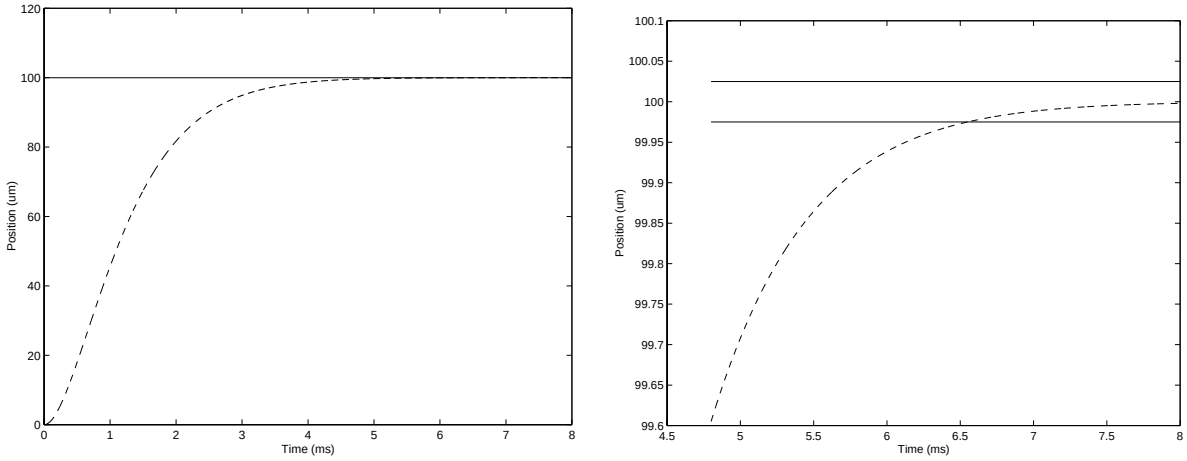

(a) (b)

Figure 4.1: Dynamics of Sled Movement in Spring Model

kg/s for $k = 300$ N/m, 0.626 kg/s for $k = 500$ N/m, and 0.743 kg/s for $k = 700$ N/m. In the experiment when mass m changes, it has different values which will be discussed later in Section 4.3.

4.3 Dynamics of Models

Figure 4.1a shows the movement of the sled x over time t from initial position to the final position of 100 μm, where the parameters are set at their default values: $F = 500 \times 10^{-4}$ N, $\lambda = 0.626$ kg/s, $m = 2 \times 10^{-4}$ kg and $k = 500$ N/m respectively. All the figures in the rest of this paper use default values of the parameters unless explicitly discussed. The two horizontal lines indicate upper and lower tolerance that determines the seek time for the spring model. These two lines are within 50 nm of each other. Figure 4.1b is a more detailed picture of the sled's dynamics when it is close to settling down, i.e., t is between 4.5 ms and 8 ms. The seek time t_{seek} for 100 μm distance is about

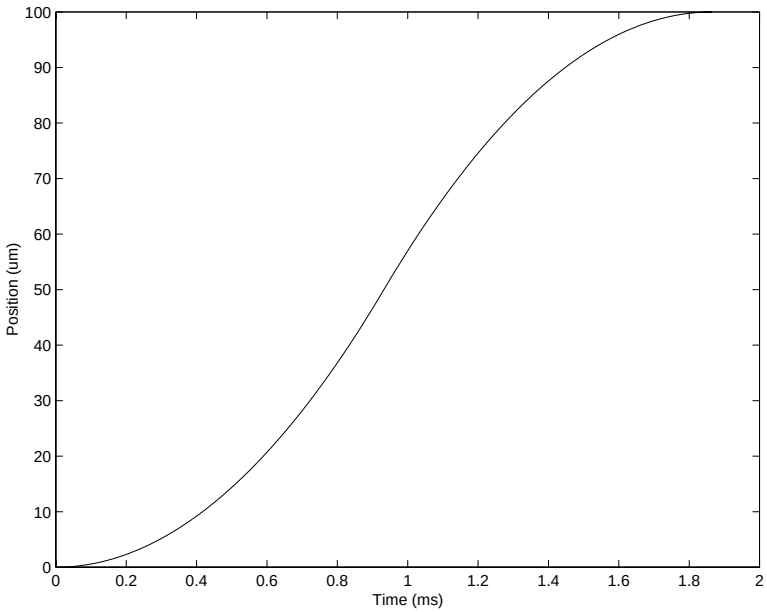

Figure 4.2: Dynamics of Sled Movement in Bang-Bang Model

6.6 ms because after that time point the sled oscillation will no longer exceed both the upper (100 μm + 25 nm) and lower (100 μm - 25 nm) tolerance lines.

Figure 4.2 displays the movement of the sled over time for the bang-bang model where acceleration equals its default value in Table 3.1 and x is 100 μm. In contrast to the dynamics of the spring model in Figure 4.1, the speed of the sled is linearly increasing during the first half of time and then is linearly decreasing during the second half. The overall shape of the dynamics curve is convex first and then concave.

Figure 4.3a plots the seek time estimated by the two modes against the distance moved. This figure indicates that for both models the seek time increases along with x^* but at a decreasing rate. Figure 4.3a also show the difference in the seek time estimated by the two models. More specifically, the seek time estimated by the bang-bang model is smaller for almost every possible value of distance x^*. When the spring model estimates that it takes

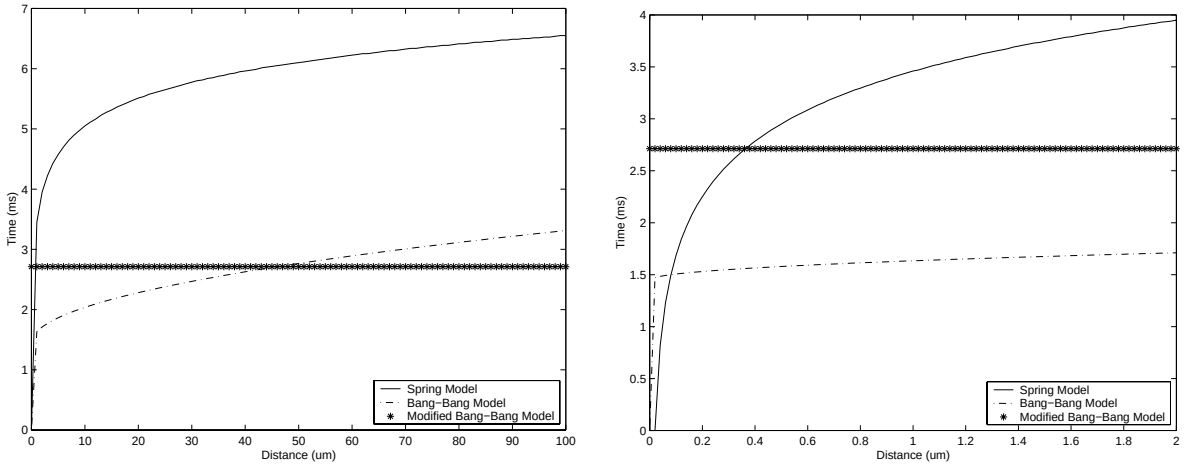

(a) (b)

Figure 4.3: Plot of Seek Time against Distance in two Models

the sled 6.6 ms to move a distance of 100 μm, the bang-bang estimates the seek time to be 3.3 ms.

Figure 4.3b gives us a zoom-in view for Figure 4.3a. We can see that when the seek distance is extremely small, the seek time estimates by bang-bang model are greater. This is because the bang-bang model assumes a constant settling down time of 1.447 ms, no matter how small the distance x^* is, which is inaccurate because positioning time approaches zero when the distance moved is infinitely small.

There is a straight line in Figure 4a and 4b, which is plotted according to Equation (3.3) but here the value of acceleration a changes. It displays the situation in which a is reset along with the variation of F according to $F = ma$. The reason for doing this is to indicate that the two models take different assumptions. In bang-bang model, acceleration is constant. For example, moving twice the distance, F in the spring model doubles. However, If a in the bang-bang doubles as well, the result would be a constant seek time

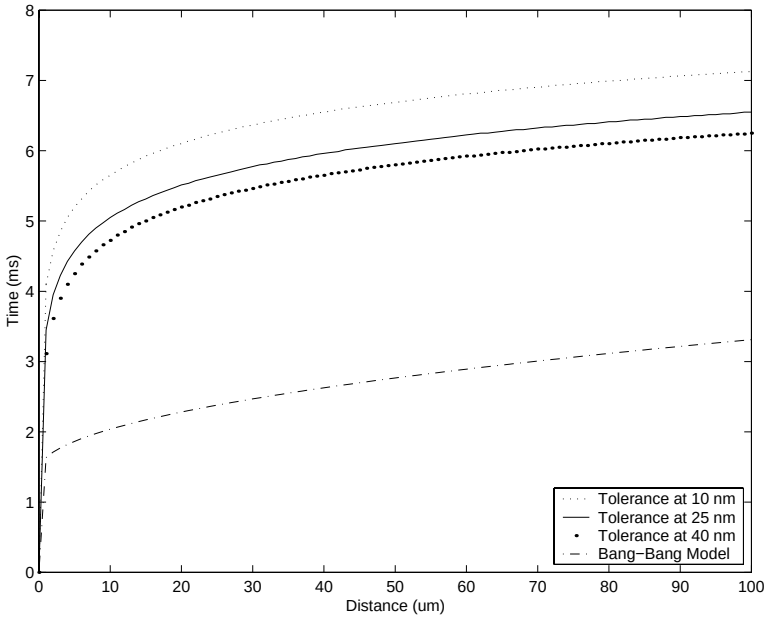

Figure 4.4: Plot of Seek Time against Distance under Different Tolerance Range

because the increase of a and x offset each other (see Equation (3.3) and Equation (3.12)).

The above experiments use tolerance of $\pm$25 nm, half of a bit width. When the tolerance varies, the seek time changes as well, as shown in Figure 4.4, in which the tolerance is set to $\pm$10 nm, $\pm$25 nm, and $\pm$40 nm. The change of the tolerance does not affect the estimated seek time for the bang-bang model which uses a fixed settle down time based upon resonant frequency ω. For the spring model, the more lenient the tolerance, the smaller is the seek time. But the estimated seek time is still much longer in the spring model than for the bang-bang model even if a lenient tolerance is applied.

Figure 4.5 studies the impact of mass parameter m upon the seek time, in which m is 1×10^{-4} kg, 2×10^{-4} kg, and 3×10^{-4} kg. For the spring model, the change of mass m leads to different values of λ according to Equation (3.10). With $k = 500$ N/m given, $\lambda = 0.445$ kg/s for $m = 1 \times 10^{-4}$ kg, $\lambda = 0.626$ kg/s for $m = 2 \times 10^{-4}$ kg which is

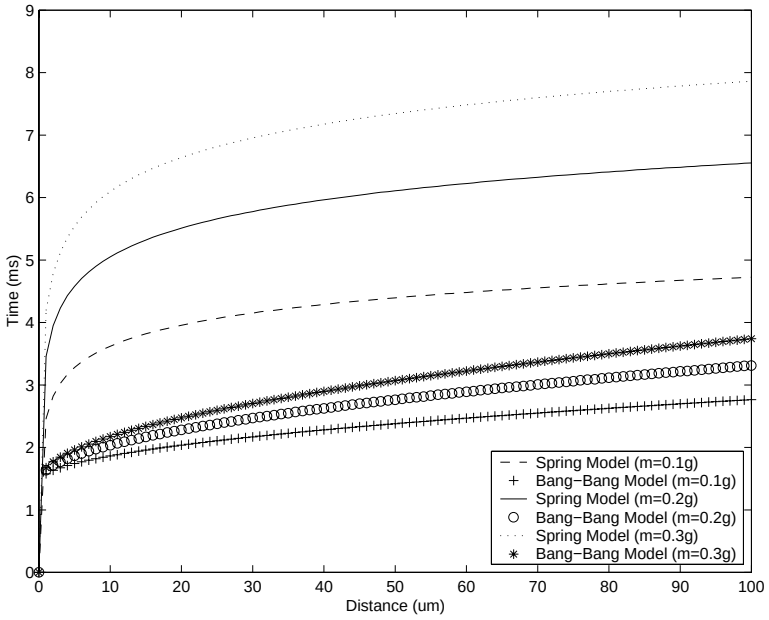

Figure 4.5: Plot of Seek Time against Distance under Different Mass

the default value, and $\lambda = 0.763$ kg/s for $m = 3 \times 10^{-4}$ kg respectively. In the bang-bang model, acceleration varies correspondingly. With $F = 230 \times 10^{-4}$ N, according to Equation (4.1), $a = 230$ m/s^2 for $m = 1 \times 10^{-4}$ kg, $a = 115$ m/s^2 (default value) for $m = 2 \times 10^{-4}$ kg, and $a = 76.7$ m/s^2 for $m = 3 \times 10^{-4}$ kg. The results indicate that for both models, with other factors unchanged, the heavier the sled, the greater the seek time, which is also consistent with Table 3.1. The seek time in the spring model is higher than that in the bang-bang model for each of the mass values.

The impact of different values of k upon seek time is shown in Figure 4.6, where k is 300 N/m, 500 N/m, and 700 N/m. For the plotting of the spring model, the parameters λ is adjusted when k changes according to the resonant frequency (ω) Equation (3.10). This is because the resonant frequency is fixed at 220 Hz for both models. Different k does not change the seek time for the bang-bang model because Equation (3.3) does not involve

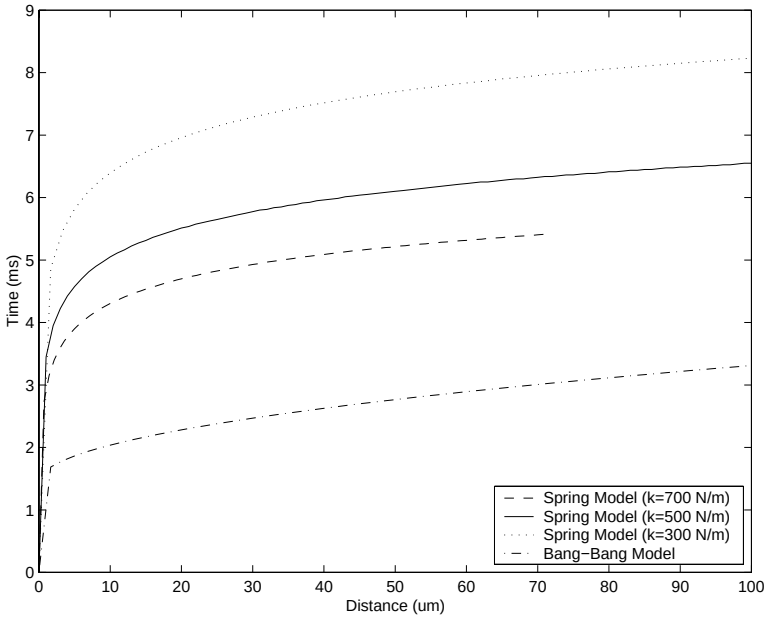

Figure 4.6: Plot of Seek Time against Distance under Different Spring Coefficients

this parameter. Figure 4.6 shows that the seek time estimated by the spring model is larger than that of the bang-bang estimates, under each value of k. When k changes, the spring model suggests that seek time t should vary, but the seek time by the bang-bang model stays the same.

In the above, we have compared the dynamics and seek times of the bang-bang model and the spring model. The spring model more precisely models the underlying mechanics of probe-based storage and has more parameters specifically describing those mechanics. With consistent physical parameters, seek times estimated by the spring model are longer than those of the bang-bang model except for very short seeks. This is because the bang-bang model optimistically uses a constant maximum acceleration, and the spring model describes the variation of acceleration in time. The spring model incorporates settle time calculation as a function of seek distance, tolerance, and resonant frequency, whereas the

bang-bang model uses a constant settle time based on estimates of these parameters. Thus, we think the spring model is more accurate than the bang-bang model.

Chapter 5

Read/Write Time for Both Models

This chapter analyzes the read/write time for both the spring and bang-bang models. In probe-based data storage system, the access time for a data request is the sum of the seek time and the read/write time. After the sled reaches the required position, the tips start reading/writing data.

Here we consider a constant read/write speed. Let us define v_{rw} to be the velocity at which tips read and write. The read/write time t_{rw} could be decomposed into four parts: actual read/write time t_A, turnaround time t_B, tip switch time t_C, and x-movement time t_D as shown in Equation (5.1).

$$t_{rw} = t_A + t_B + t_C + t_D \tag{5.1}$$

In Equation (5.1), t_A is derived by dividing the total distance traveled by the sled in reading/writing with the velocity v_{rw}; t_B is calculated by multiplying the total number of turnarounds with the time used on one turnaround; t_C is obtained by multiplying the

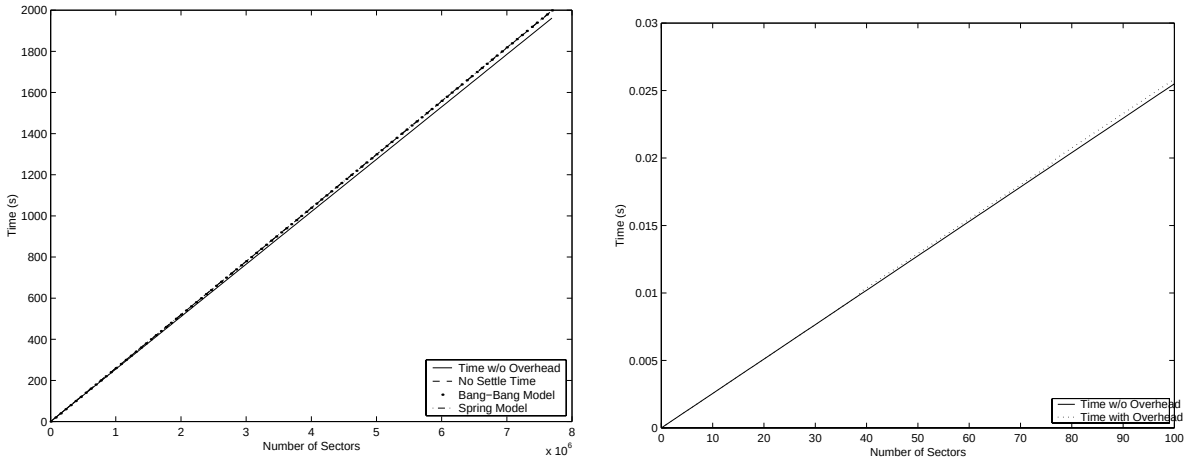

(a) (b)

Figure 5.1: Read/Write Time

number of tip switches with the time spent on one tip switch; and t_D is also calculated accordingly.

In Equation (5.1), turnaround time t_A is necessary because the sled's direction may be reversed during the process of reading/writing. And t_B is the time needed for the activation and switch of tips. In our probe-based device, only one row of tips is active at a time. After one row finishes reading/writing data, the next row is activated. x-movement is required for the sled to move from one column of bits to the next column in x-dimension which is a seek activity and will involve the mechanics discussed in Chapter 3.

5.1 Experiments of Read/Write Time

Equation (5.1) is used to calculate the read/write time. The calculations of the first three terms are the same for the spring and the bang-bang models. But for the last term, *i.e.*, the x-movement time, the two models take different approaches because we must

reposition the sled from one column of bits to the next one. According to the dynamics models developed in Chapter 3, the time on one movement in x-dimension can be calculated by using the following three methods. Here the distance moved is 50 nm, one bit size.

- Using bang-bang model and omitting the settling down time t_{settle} because we think it may not take a constant time of 1.447 ms to settle down for such a small distance of 50 nm. The result is 0.0417 ms.
- Using the bang-bang model with the settling down time. The time is 1.49 ms.
- Using the spring model, which depends upon parameters values. Given $m = 2 \times 10^{-4}$ kg, $\lambda = 0.74$ kg/s, $k = 700$ N/m, and $F = 3.5 \times 10^{-5}$ N, the result is 0.893 ms.

The x-movement time obtained through the above three methods is different. In our experiments, we take $v_{rw} = 0.01$ m/s, $a = 115$ m/s^2. According to first-order mechanics, time for one turnaround is $2 \times \frac{v_{rw}}{a} = 0.174$ ms. The tip switch time is assumed to be zero because it takes almost zero time to activate and switch tips.

Figure 5.1a plots the read/write time needed against the number of sectors processed when considering four cases: time without including those spent on turnaround and x-movement; total read/write time with the x-movement time using bang-bang model but omitting settle down time; total read/write time with the x-movement time using bang-bang model; total read/write time with the x-movement time using spring model. The

number of sectors ranges from 0 to $7,692,000$ which is the maximum number that the sled can accommodate per request according to our design. We assume there are 512 bytes per sector in the experiments. The figure shows that the read/write time for $7,692,000$ sectors is around 2000 seconds. Accordingly, we get the throughput 1.9 Mbyte/second which is consistent with the access rate of $100 - 200$ Kbit/second per tip (there are 100$\times$100 tips in the design).

Figure 5.1a shows that read/write time increases linearly with the number of sectors. The majority part of the time is spent on actual reading/writing. Because the overhead time is quite small, the total time plotted by using three different x-movement time calculations is similar(the three lines overlap).

Figure 5.1b displays the results with much less number of sectors: 1, 2, ..., up to 100. Here we plot two lines representing the read/write time with or without overhead (turnaround and x-movement). Being identical to Figure 5.1a, this figure suggests that overall linear relationship still holds even though small amount of data are processed through the probe-based system.

Chapter 6

Conclusion

This thesis develops the spring model, a new approach to analyze the dynamics of sled movement in probe-based storage system by using classical physics and mechanics theory, and identifies major factors that contribute to this process.

The spring model is different from the previous bang-bang model in probe-storage system modeling because it describes how acceleration varies continuously in time. It models the physical system at a lower level, and can accommodate a wider range of parameters. It provides a more accurate calculation of the settle time, based on these underlying physical and mechanical parameters. Higher-level system design decisions depend upon accurate models of low-level behavior, and we have described important differences in the two modeling approaches that warrant further investigation.

While we believe the spring model is a promising approach for the new generation of probe-based storage system, there are several research areas that could be examined

further. Firstly, the assumption of external F being independent of t can be reconsidered because the electric voltage of the probe-based storage system may vary with time. So it is interesting to understand how the alternation of this assumption may change the dynamics process and seek time estimation. Secondly, we need to study how the two models estimate the read/write time when considering the repositioning mechanics involved in x-dimension movement from one column of bits to the next one. And thirdly, it needs further examination on how the estimated seek time by the two models differ in simulations using application benchmarks.

Bibliography

[1] C. Brown. Microprobes promises a new memory option. *E.E. Times*, 1998.

[2] L. R. Carley. www.chips.ece.cmu.edu, 1999.

[3] S. H. Charap, P. L. Lu, and Y. He. Thermal stability of recorded information at high densities. In *IEEE Transactions on Magnetics, vol. 33*, 1994.

[4] M. Despont, J.Brugger, U. Drechsler, U.Durig, W. Haberle, M. Lutwyche, H. Rothuzen, R. Stutz, R. Widmer, H. Rohrer, G. Binnig, and P. Vettiger. VLSI-NEMS chips for AFM data storage. In *Technical Digest. IEEE International MEMS 99 Conference. Twelfth IEEE International Conference on Micro Electro Mechanical Systems*, 1999.

[5] J. L. Griffin and S. W. Schlosser. Characteristics and applications of ubiquitous smart storage. Technical report, Laboratory for Computer Systems, Carnegie Mellon University (unpublished draft), 1999.

[6] J. L. Griffin, S. W. Schlosser, G. R. Ganger, and D. F. Nagle. Modeling and per-

formance of MEMS-based storage devices. In *Proceedings of ACM SIGMETRICS 2000*, 2000.

[7] G.T.Sincerbox and ed. Selected papers on holographic storage, vol.ms 95 of SPIE milestone series. In *Internal Society for Optical Engineering*, 1994.

[8] W. Hauser. *Introductory Mechanics*. Northeastern University Textbook Program, 1987.

[9] A. Hudson and R. Nelson. *University Physics*. Harcourt Brace Jovanovich, Inc., 1982.

[10] W. A. Johnson and L. K. Warne. Electrophysics of micromechanical comb actuators. In *Journal of Microelectromechanical Systems*, 1995.

[11] H. J. Mamin, B. D. Terris, L. S. Fan, S. Hoen, R. C. Barrett, and D. Rugar. High-density data storage using proximal probe techniques. In *IBM Journal of Research and Development*, 1995.

[12] M. Mehregany, W. H. Ko, A. S. Dewa, and C. C. Liu. Introduction to MEMS systems and the multiuser mems processes. Technical report, Electronics Design Center, Department of Electrical Engineering & Applied Physics, Case Western Reserve University, 1993.

[13] D. Psaltis and G.W.Burr. Holographic data storage. In *IEEE Computer*, 1998.

[14] S. Redfield and J. Willenbring. Holostore technology for higher levels of memory hierarchy. In *Eleventh IEEE Symposium on Mass Storage Systems,* 1991.

[15] C. Ruemmler and J. Wilkes. Modeling disks. Technical Report HPL-93-68, Hewlett Packard Laboratories, 1993.

[16] S. W. Schlosser, J. L. Griffin, D. F. Nagle, and G. R. Ganger. Filling the memory access gap: A case for on-chip magnetic storage. Technical report, School of Computer Science, Carnegie Mellon University, 1999.

[17] Ya. B. Zeldovich and A. D. Myskis. *Elements of Applied Mathematics*. MIR Publishers Moscow, 1976.

[18] X. Zhang and W.C. Tang. Viscous air damping in laterally driven microresonators. In *Sensors and Materials*, 1995.

Appendix A

Solution to the Second-Order Differential Equation

This appendix provides the solution for the second-order differential Equation (3.5) where m, λ, and k are parameters. The deduction of solution closely follows Zeldovich *et al.* [17]. In many aspects, the properties of this equation are similar to those of first-order homogeneous linear equations. For instance, it is easy to verify that if $x_1(t)$ is a particular solution of (3.5), then also is $Cx_1(t)$, where C is any constant; that if $x_1(t)$ and $x_2(t)$ are two particular solutions of (3.5), then their sum $x(t) = x_1(t) + x_2(t)$, is also a solution of that equation.

From the above, then if we have found two particular solutions $x(t) = x_1(t)$ and $x_2(t)$, then their linear combination,

$$x(t) = C_1 x_1(t) + C_2 x_2(t) \tag{A.1}$$

where C_1 and C_2 are two arbitrary constants, is also a solution of that equation. The general solution of a second-order differential equation is obtained via two integrations which results in two arbitrary constants. Therefore the expression (A.1) can be used as the general solution of Equation (3.5). It is obvious that C_1 and C_2 should not be linearly dependent with each other.

In order to find the two independent solutions of Equation (3.5), we use Euler's approach which takes the form

$$x(t) = e^{pt} \tag{A.2}$$

where p is a constant to be found. Substituting (A.2) into (3.5) we get the following characteristic equation

$$mp^2 + \lambda p + k = 0 \tag{A.3}$$

In solving the above equation, there are different cases, depending upon the sign of the discriminant:

$$D = \lambda^2 - 4mk$$

If the friction is great, namely, if $\lambda^2 > 4mk$, then (A.3) has real roots:

$$p_{1,2} = \frac{-h \pm \sqrt{\lambda^2 - 4mk}}{2m}$$

Let $p_1 = -a$ and $p_2 = -b$. Then, on the basis of (A.1) and (A.2), we get the general solution of (3.5) in the form of Equation (3.7). According to this equation, in the case of

strong friction, the deviation of a point from the equilibrium tends to zero exponentially with t without oscillations.

If the friction is small, that is to say, if $\lambda^2 < 4mk$, then (A.3) has imaginary conjugate roots:

$$p_{1,2} = \frac{-h}{2m} \pm i\sqrt{\frac{k}{m} - \frac{h^2}{4m^2}} = -r \pm i\omega$$

where r and ω are represented in Equation (11) and (12). Then we get the general solution (A.1)

$$x = C_3 e^{-rt+i\omega t} + C_4 e^{-rt-i\omega t} = e^{-rt}(C_3 e^{i\omega t} + C_4 e^{-i\omega t}) \tag{A.4}$$

The terms $C_3 e^{i\omega t}$ and $C_4 e^{-i\omega t}$ are periodic functions with frequency ω. Applying Euler's formula, we could rewrite Equation (A.4) into Equation (3.13).

In the case when $\lambda^2 = 4mk$, we have two equal real roots, the solution will become:

$$x = C_5 e^{-at} + tC_6 e^{-at}$$

Here C_5 and C_6 are two arbitrary constants.